Assessing quality and purity of MoS_2 nanosheets by diffuse reflectance IR spectroscopy

To cite this article: Tim Nowack *et al* 2025 *2D Mater.* **12** 045021

2D Materials

PAPER

Assessing quality and purity of MoS_2 nanosheets by diffuse reflectance IR spectroscopy

Tim Nowack[1], Lorenzo Bastonero[2], Timm Knickrehm[1], Tian Carey[3], Oran Cassidy[3], Jonathan N Coleman[3], Zdenek Sofer[4], Kevin R Synnatschke[3,5], Nicola Marzari[2,6,7] and Claudia Backes[1,*]

[1] Physical Chemistry of Nanomaterials and CINSaT, University of Kassel, Heinrich-Plett-Str. 40, 34132 Kassel, Germany
[2] U Bremen Excellence Chair, Bremen Center for Computational Materials Science, and MAPEX Center for Materials and Processes, University of Bremen, 28359 Bremen, Germany
[3] School of Physics, CRANN & AMBER Research Centres, Trinity College Dublin, D02 E8C0 Dublin, Ireland
[4] Department of Inorganic Chemistry, University of Chemistry and Technology Prague, Technická 5, 166 28 Prague 6, Czech Republic
[5] Technical University of Dresden, Center for Advancing Electronics Dresden (cfaed) and Faculty of Chemistry and Food Chemistry, 01062 Dresden, Germany
[6] Theory and Simulation of Materials (THEOS), and National Centre for Computational Design and Discovery of Novel Materials (MARVEL), École Polytechnique Fédérale de Lausanne (EPFL), CH—1015 Lausanne, Switzerland
[7] PSI Center for Scientific Computing, Theory, and Data, and National Centre for Computational Design and Discovery of Novel Materials (MARVEL), 5232 Villigen, PSI, Switzerland
* Author to whom any correspondence should be addressed.

E-mail: backes@uni-kassel.de

OPEN ACCESS

RECEIVED
28 August 2025

REVISED
29 September 2025

ACCEPTED FOR PUBLICATION
9 October 2025

PUBLISHED
22 October 2025

Keywords: 2D materials, transition metal dichalcogenides, MoS_2, solution processing, IR spectroscopy

Supplementary material for this article is available online

Abstract

Liquid-phase processing is increasingly used to produce thin films and composites from nanomaterials, including 2D nanosheets derived from van der Waals crystals. However, an inherent problem is the exposure of the nanomaterial to organic compounds from the environment—solvents, intercalants, and stabilizers—which can adsorb and potentially degrade device performance, especially at electrode interfaces. For conventional washing methods it is often challenging to confirm complete removal, as these residues are difficult to detect spectroscopically. Here, we use diffuse reflectance infrared (IR) Fourier transform spectroscopy to analyze freeze-dried 2D MoS_2 nanosheets produced via various exfoliation methods. First-principles calculations predict IR spectral shifts corresponding to nanosheet thickness in the few-layer regime (<10 layers), which were confirmed experimentally. We demonstrate that centrifugation effectively removes small-molecule surfactants (e.g. 2 g l^{-1} sodium cholate or sodium dodecyl sulfate) used in liquid-phase exfoliation, while residues persist in MoS_2 sonicated in NMP or electrochemically-exfoliated samples. This work provides a protocol to improve washing or monitor chemical modifications and highlights that IR-active vibrational modes, accurately predicted from first principles, can serve as a tool to determine 2D material layer numbers.

1. Introduction

The production of 2D nanomaterials involves various organic molecules, such as residues from adhesive tape or polymeric stamps after mechanical exfoliation, solvents, or stabilizing surfactants/polymers after liquid-phase exfoliation (LPE), or additional intercalants after chemical or electrochemical exfoliation (EE) [1–6]. These molecules can initially remain on the newly created surfaces of the 2D nanomaterials. From a chemical perspective, residual organic molecules from 2D material processing can hinder or interfere with further controlled surface modification, such as functionalization reactions. From a physical perspective, these molecules can induce doping effects and other undesired/uncontrolled effects on the performance of the materials in electrical devices [7, 8] and present a barrier in the fabrication of heterostructures with van der Waals contact between the 2D materials. Therefore,

identification and quantification of these species during the process chain is crucial. Traditionally, Raman and x-ray photoelectron spectroscopy (XPS) are among the most utilized spectroscopic techniques to characterize these 2D nanosheet surfaces [9]. However, very thin adlayers of contaminants can often not be detected or quantified, and highly resolved tools such as time-of-flight secondary ion mass spectrometry (TOF-SIMS) are necessary to prove their ubiquitous presence [2]. This is because Raman spectroscopy on common 2D materials is often based on resonant excitation which enhances the signal of the 2D material relative to non-resonant surface adsorbates on the one hand. On the other hand, surface adsorbates are typically carbon-based materials which are hard to identify and quantify precisely in XPS due to the simultaneous presence of adventitious carbon.

Another potential technique to monitor organic species on the surface of nanomaterials is infrared (IR) spectroscopy which probes vibrational transitions in organic molecules in the mid-IR (MIR) spectral region. This is typically measured in total reflectance or transmission. In the context of 2D materials, IR spectroscopy has primarily been used to identify organic functional groups grafted (covalently) on graphene or MoS_2 scaffolds, or to track MoS_2 catalyzed organic reactions [10–13]. However, when applied to inorganic nanomaterials such as MoS_2, no information on the nanomaterial itself is contained in the MIR region, as IR-active vibrations of MoS_2 are usually located in the far-IR (FIR) which is not accessible by routine measurements due to instrument restrictions (e.g. window-material, unsuitable refractive index of crystal in total reflection). These can be overcome also with commercial benchtop spectrometers with minor modifications in the setup, such as a diffuse reflectance accessory in combination with CsI matrix material (for more details see S1). This allows the measurement down to ~370 cm^{-1}, where for example Mo-S vibrations were predicted [14]. In few experimental reports, these vibrations have indeed been observed experimentally, but not discussed or analyzed in detail (see SI of [6, 15]). In principle, through a MIR-FIR spectrum organic surface adsorbates/functional groups can be probed relative to the MoS_2 which would greatly facilitate comparative studies and allow a semi-quantitative assessment. Importantly, the method probes the ensemble of all nanosheets present in the sample which allows to assess a robust average. Another key advantage of this technique is that it is low-cost, can be performed under ambient conditions, and has the potential to be applied to other material scaffolds. For examples, see table S2. Moreover, experimentally observed IR active modes can readily be correlated to calculated vibrations from first-principles calculations. This is more complicated in the case of Raman spectroscopy. While being the commonly used vibrational spectroscopy for 2D materials, it suffers from resonance effects and higher order Raman scattering which is challenging to calculate [16]. To date, no systematic IR spectroscopy studies on MoS_2 have been carried out and it remains unclear, to which extent the observed modes contain information on material properties such as layer number.

In this work, we address these points. We established a protocol to reliably measure MIR-FIR spectra in diffuse reflectance infrared Fourier transform (DRIFT) spectroscopy. We applied this to MoS_2 nanosheets from sonication-based LPE and EE. Using first-principles calculations of the thermodynamically stable and naturally abundant 2H MoS_2 of layer numbers up to 9 (including bulk), we correlate spectral changes to nanosheet layer number. The excellent agreement between theory and experiment suggests that density-functional theory (DFT) is capable of calculating thickness-dependent changes with great precision. Further, we conducted in depth studies to trace organic surface adsorbates such as solvent and surfactant residues on the nanosheet surface and used the semi-quantitative MIR-FIR spectra to develop efficient purification protocols for LPE and EE MoS_2. We find that (i) common small molecule surfactants in LPE (such as sodium cholate (SC) can be widely removed by washing with water (ii) sonication in N-methyl-2-pyrrolidone (NMP) results in surface adsorbates that cannot be removed (iii) EE nanosheets are difficult to purify due to the use of dimethyl formamide (DMF) in combination with a polymeric stabilizer commonly applied to exfoliate and stabilize the intercalated crystals. Here, more extensive washing is required, ideally combining washing with small molecule surfactants. The purified samples are of interest for applications in electronics where control over doping is crucial. The characterization procedure elaborated is general and can be applied to covalently functionalized MoS_2.

2. Results and discussion

2.1. Infrared modes of MoS_2 at different thickness

Within this work, the utilized exfoliation methods commonly maintain the naturally abundant 2H polymorph of MoS_2 during processing [17]. DFT calculations on IR active intrinsic 2H MoS_2 modes published previously typically focus on bulk and monolayer (ML) materials predicting modes below 500 cm^{-1} in both cases, which is known as the FIR region [14, 18]. The dominant bands are referred to as shear (around 383 cm^{-1} in bulk, experimentally) and breathing mode (around 469 cm^{-1} in bulk, experimentally) [19]. This implies that the intrinsic MoS_2 material vibrations can be measured alongside (but not overlapping with) the organic molecules'

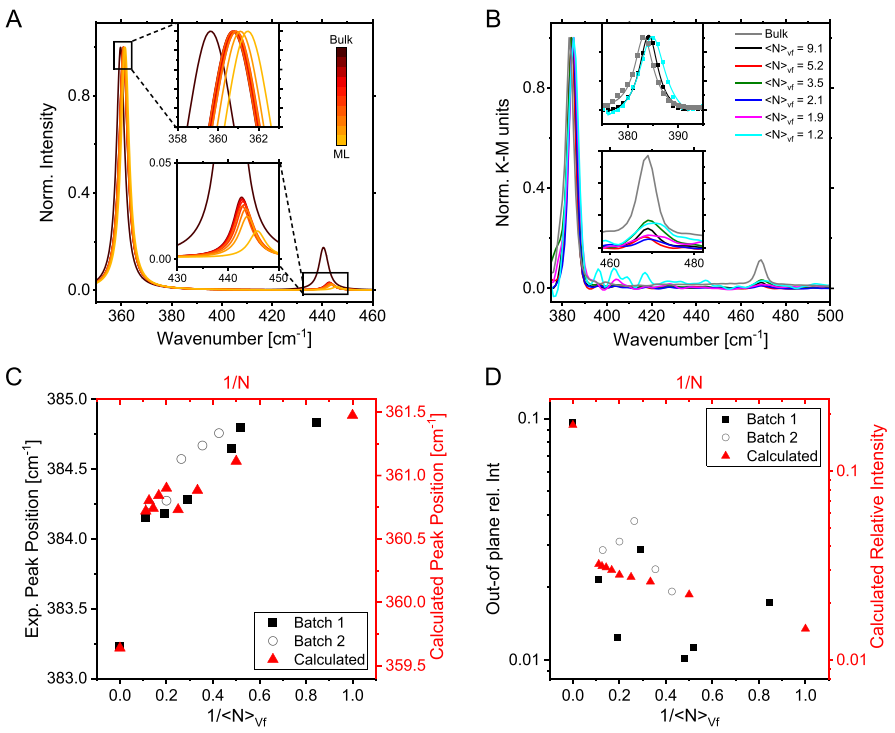

Figure 1. (A) Calculated far-infrared spectra of 2H-MoS_2 for bulk and layer numbers between 1–9, normalized to the shear mode of MoS_2. The insets show enlarged peak ranges. (B) Diffuse reflectance FTIR (DRIFT) spectra of liquid-phase exfoliated and size-selected nanosheet ensembles with different volume-fraction weighted layer number $<N>_{Vf}$. All spectra were normalized to the shear mode of MoS_2. For additional spectra, see figure S3 (C) Peak centers of Lorentzian fits of the shear mode of MoS_2 plotted against the reciprocal of $<N>_{Vf}$. On a second scale (red) theoretical peak positions are indicated. (D) Intensity of breathing mode of MoS_2 (relative to the shear mode) plotted against the reciprocal $<N>_{Vf}$. Theoretical peak intensities are indicated on a second scale (red).

vibrations—typically found in the mid-IR up to ~4000 cm^{-1}. To assess the suitability of our setup to reliably measure the FIR vibrations, we first produce a range of samples with different average layer number using LPE in combination with size selection and compare the results to calculated spectra. In order to cover the experimentally expected average thicknesses [4], here first-principle calculations of IR spectra based on DFT [20] were performed on bulk and layer numbers between one and nine, and normalized to their maximum intensity (figure 1(A)) to understand the effects of nanosheet dimensions on IR spectra.

Going from bulk to ML, a shift to higher wavenumber of about 2 cm^{-1} is predicted for the intra-layer shear MoS_2 mode with the most significant shift already between bulk and nine layers (9 l). The softening of the vibrational frequency is attributed to the inter-layer friction (i.e. van der Waals interaction) between the layers, which becomes effectively larger for increasing number of layers. This observation is analogous to the well-known trend for pure shear and breathing inter-layer Raman modes [19], where analytical models can be developed to capture low frequency (<100 cm^{-1}) oscillations. In addition, a striking change in the breathing mode can be seen, manifested as a drop in relative intensity compared to the shear mode. Again, this change is most pronounced going from bulk to few layers (here 9 layers). In the few to ML regime, this decrease further progresses (see inset figure 1(A)) and is accompanied with a shift in peak position from bulk to ML from about 440–446 cm^{-1}. In summary the calculated spectra predict (i) a shift of the intra-layer shear-mode and (ii) a decrease in relative intensity of the breathing mode. As discussed below this is experimentally confirmed.

To study such modes using benchtop IR spectrometers, first, a suitable setup is required (see S1). We identified DRIFT spectroscopy using CsI as matrix material as most promising as summarized below. Secondly, sufficiently large amounts of material are needed to allow for sufficient signal/noise ratio (typically on the milligram scale). Thirdly, additional chemical species interfering in the spectrum must be minimized, i.e. additives or utilized solvents must be removed if they have bands in the FIR. Finally, control of average nanosheet dimensions is crucial to reliably compare experiment and theory. Therefore, we chose sonication-based LPE of MoS_2 in H_2O/ SC, a production technique yielding sufficiently high dispersed mass of MoS_2 as well as distributions of nanosheet

dimensions that range down to MLs. These distributions can be narrowed and controlled by liquid cascade centrifugation (LCC) [21] which results in efficient size selection. From the obtained fractions of nanosheets with different sizes and thicknesses, average values of the dimensions can be extracted using UV–VIS extinction spectroscopy [22]. To minimize spectral interference by contaminants, a centrifugation based washing was performed and the solvent removed by freeze-drying (see Methods) to avoid ordered restacking and potential degradation compared to drying in air at elevated temperatures [23].

DRIFT spectroscopy was selected as a measurement setup to avoid potential issues arising from other commercial setups such as transmission measurement with KBr pellets or attenuated total reflection (ATR). In the case of KBr pellets, the intrinsic absorbance of KBr in the FIR poses a problem in addition to turbidity of KBr pellets from failure-prone preparation when water cannot be fully excluded. In ATR setups, it is required that the refractive index of the ATR crystal is larger than that of the sample which is not guaranteed in the case of 2D materials in general and MoS_2 specifically. For the measurement, the freeze-dried nanosheet powder is mixed with CsI as reflective matrix material and subjected to the measurement in a small beaker without further treatment. This method is simple, avoids heat and can in principle be carried out under inert conditions. It is thus expected to be broadly applicable to many 2D materials, also those prone to degradation in the presence of oxygen, water or heat.

The spectra from freeze-dried size-selected fractions of LPE MoS_2 are shown in figure 1(B). Spectra from a second batch of similar exfoliation and size selection are shown in figure S3C. Both IR active vibrations are discerned at ∼384–385 cm^{-1} and ∼469 cm^{-1}, respectively. The intensity was converted to Kubelka–Munk units (see methods) and normalized to the more intense intralayer shear mode. In the insets in figure 1(B) both characteristic peaks are shown: For the shear modes Lorentzian functions were fit to the data points obtained, to extract peak positions. A shift similar in magnitude to theoretical predictions is observed for the shear mode as visualized in figure 1(C), where we plot the peak position as a function of inverse (average) layer number, N (see S3 for spectra and N (or strictly speaking $\langle N \rangle_{Vf}$) determination). This representation is chosen to allow the addition of the data point of bulk MoS_2 at $1/N = 0$. Note that there is a shift in phonon frequency between DFT calculations and experiments, which could be related to the choice of the functional, which is in general expected to predict softer phonon frequencies [24–28]. Moreover, the calculations do not include any type of temperature, substrate, or presence of defects effects, that might hinge on the accuracy of the peak positions. However, the relative shift agrees very well. While the shift is small for MoS_2, the good agreement is encouraging, as it suggests that theory can be used to identify layered materials with more significant layer-number dependent IR-active response.

In addition to the shift of the shear mode, the breathing mode decreases in relative intensity compared to the shear mode drastically—as also expected from theory. We note that calculated breathing mode intensities and peaks depend strongly on how the dielectric environment is modeled (see Methods). This sensitivity is mirrored experimentally: layer-averaged spectra exhibit greater noise in breathing than shear modes. This makes it difficult to reliably fit peaks to for example extract peak positions due to the low signal/noise ratio. To nonetheless visualize the decrease in relative intensity, the relative Kubelka–Munk units at 469 cm^{-1} were subtracted from the ones at 478 cm^{-1} and plotted on the log scale as function of inverse layer number, again in comparison with theory (figure 1(D)). While predicted peak shifts describe experimental data very well for the shear mode, a scattered trend can be observed for the intensity behavior of the breathing mode: Even though low signal/noise ratio is a clear contribution to this issue, it should also be considered that residual bulk like particles can remain in dispersions even after size-selection and cause additional scatter in the data as the intensity of bulk MoS_2 is∼1 order of magnitude larger than that of few-layered sheets. Any trace amounts will thus have a large effect on the intensity. Thus, for correlating IR features with layer number, analysis of the shear mode is superior to that of the breathing mode.

Overall, the good agreement between experiment and first-principles calculations verifies that DRIFT Spectroscopy of the freeze-dried samples is a suitable methodology. The random restacking in freeze-drying does not substantially alter effectively observed nanosheet dimensions, i.e. trigger defined nanosheet restacking or degradation. Therefore, the utilized approach appears suitable to further process and study other 2H MoS_2 dispersions in the same way and use the shear mode around 384 cm^{-1} as a reliable guide for MoS_2 content in each specimen to enable a semi-quantitative analysis.

2.2. Effect of MoS_2 surface area to study molecular adsorption

The newly created nanosheet surfaces during LPE are highly susceptible to aggregation and degradation, requiring stabilization against these processes [29, 30]. Initially, a broad range of organic solvents and later solvent blends were shown to be effective for this purpose [31, 32]. Also surfactants in aqueous solution as well as polymers in organic solutions have been found to be suitable for stabilizing the nanosheets [3, 21]. However, in all these cases, organic molecules

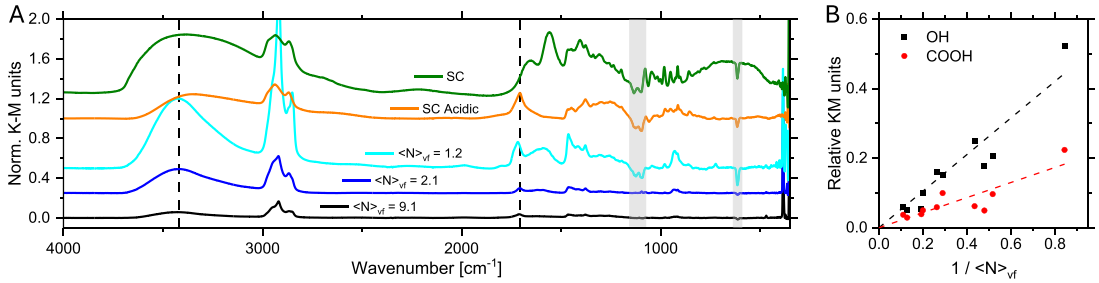

Figure 2. (A) Measured DRIFT spectra in MIR of size-selected LPE MoS_2 nanosheet powders from sonication in aqueous SC normalized to the shear mode of MoS_2. Grey boxes cover areas of the CsI matrix. The spectrum of freeze-dried (acidic, orange) solution of SC (green) is given for reference. (B) Relative KM-units at characteristic wavenumbers of cholic acid (highlighted by dashed lines in figure 2(A)) plotted against MoS_2 $<N>_{Vf}$. Dashed lines in figure 2(B) are linear fits through the origin. Full sets of associated MIR spectra can be found in figure S5.

come into contact with the MoS_2 surfaces, which must be removed eventually for many applications [7, 8]. Here, we will use DRIFT Spectroscopy to track the presence of these solvents and stabilizers. Fortunately, mid-IR spectra for a vast number of solvents, surfactants, and other additives are readily available in databases, facilitating the analysis of the spectra.

In our first example, we exfoliated MoS_2 nanosheets in an aqueous medium with SC as surfactant through sonication-assisted LPE and performed size selection through LCC. The FIR spectra region of the samples is discussed above. In the following, we analyze the MIR region to track the presence of the surfactant as a function of average nanosheet layer number and hence surface area. This mainly serves the purpose to identify the most suitable nanosheet thickness range for this kind of measurement. On the one hand, the relative intensity of the MIR vibrations of the surfactant should increase with increasing surface area, i.e. fractions containing thin nanosheets should be ideal. On the other hand, as mentioned above, a sufficient quantity of nanosheets is required for the measurement to optimize the signal/noise ratio. Since the mass of small and thin nanosheets is lower than of large/thick nanosheets [33], it is important to find a compromise between the two aspects for subsequent work.

The FIR-MIR DRIFT spectra of a subset of size-selected fractions are shown in figure 2(A). Spectra were normalized to the shear Mo-S mode to reference for the amount of nanosheet mass in the beam. Since the only organic molecule used in the aqueous process was the surfactant, bands from SC are expected. The reference spectrum is displayed as a green trace, figure 2(A). Notably, the band typically assigned to the deprotonated carboxyl group around 1655 cm^{-1} appears shifted in the LPE MoS_2-SC spectra (black, blue & cyan). IR measurements of protonated surfactant (figure 2(A), orange trace) suggest that the dominant adsorbed species is cholic acid (~1707 cm^{-1}). We rationalize this through reference experiments showing a decreasing pH of aqueous MoS_2 dispersions during the sonication process (see figure S4).

The spectral contribution of this band, as well as the band associated with OH groups (~3400 cm^{-1}), appears to increase with available nanosheet surface area (i.e. decreasing nanosheet thickness) and hence adsorbed surfactant [34] as anticipated. The region associated with saturated alkyl vibrations (2900–3000 cm^{-1}) also shows a monotonous increase. However, it is worth noting that adventitious carbon might contribute to this band, and therefore it was not further considered here [2]. For further analysis, the intensity of these bands in the MIR, relative to the Mo–S shear mode, is plotted as a function of inverse average layer number (figure 2(B)). Data from different batches is included, the spectra are shown in the SI. The lines serve as a guide for the eye and represent fits through the origin suggesting a correlation between the Kubelka–Munk units of the respective bands and the organic residues adsorbed to the surface, in spite of scatter in the data. We attribute the scatter in the data to variations in sample preparation across different batches due to the unclear impact of changes in the pH because the MIR spectra (SI, figure S5) of different batches show a different signature especially in the region of the carbonyl stretching vibration.

Overall, the data on the size-selected fractions of MoS_2 produced by sonication-assisted LPE allowed us to identify the presence of residual surfactant, in spite of some centrifugation-based washing with water to remove loosely physisorbed surfactant (see methods). From the data, we infer that an average layer number well below 10 is suitable to track the presence of surfactants as surface adsorbates. In the following, we will use centrifugation conditions targeting this thickness range in combination with maximized mass (see methods) informed by our predictive size selection model [35]. It is worth noting that for samples prepared in a similar way, Raman spectroscopy did not show noticeable surfactant-related

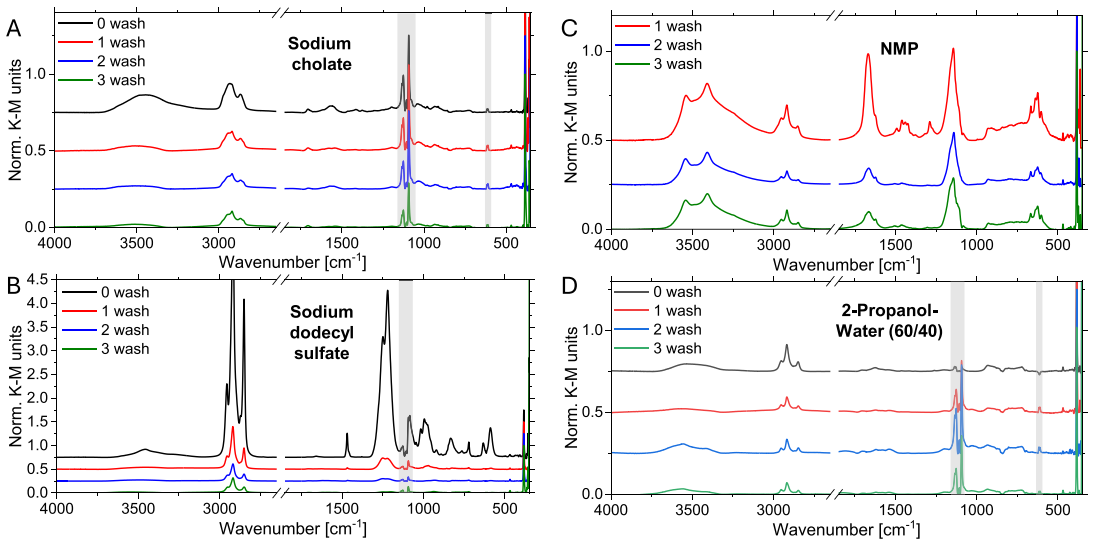

Figure 3. Measured DRIFT spectra in mid-infrared of exfoliated and size-selected MoS_2 nanosheet powders. Exfoliation was done in (A) H_2O/SC, (B) H_2O/SDS, (C) N-Methyl-2-pyrrolidone, (D) 2-Propanol/H_2O (60/40). Different traces represent different number of washing steps (sedimentation in centrifuge & redispersion in H_2O or IPA in case of NMP). All spectra are normalized to the shear mode of MoS_2.

bands, likely due to the resonant excitation of MoS_2 and hence enhanced intensities of Mo–S vibrations over non-resonant organic molecules. This makes the presented method a valuable tool for monitoring nanosheet surface purification for exfoliated materials obtained by different liquid processing, as we will address below.

2.3. Removal of residues from sonication-assisted LPE

As demonstrated above, LPE in H_2O/SC is accompanied by residual surfactant molecules adsorbed on the surface as evidenced by DRIFT spectroscopy. Therefore, in the following, we compare DRIFT spectra after exfoliation using different surfactants (SC and sodium dodecyl sulfate, SDS) as well as pure solvents (NMP and a solvent blend of isopropanol/water—IPA/H_2O), i.e. without additional surfactant. The goal is to find suitable post-exfoliation processing through centrifugation-based washing to minimize the presence of residual surface adsorbates. The 'washing' procedure involves centrifugation at a speed and time sufficient to allow nanosheets to sediment. The supernatant is decanted and discarded, while the nanosheet sediment is redispersed in fresh solvent and subjected to another centrifugation under the same conditions. When stabilizers are only weakly bound to the surface, they should be removed through desorption in this way. For further reference, DRIFT spectra of pure solvent/surfactants can be found in the SI (figure S7). The respective MoS_2 size fractions were of average-size &—thickness in each case, i.e. large and thick as well as small and thin nanosheets were removed. UV–VIS extinction spectra can be found in figure S6. From spectroscopic metrics [22], we assess the average volume-fraction weighted MoS_2 layer number to be ∼6 (based on the spectra in SC).

In the presented spectra (figure 3), normalization was again performed relative to the Mo-S shear mode. In such a representation, the relative Kubelka–Munk units should scale with the amount of additional organic molecules as well as their IR oscillator strength. For the case of MoS_2 exfoliated in SC (figure 3(A)), the relevant bands were already mentioned above. They appear relatively weak, but well discernible, for the given size fraction after transfer of the dispersion to water (0 wash) and subsequent freeze-drying. Additional centrifugation-based washing with water indeed reduces the relative Kubelka–Munk units, particularly for the bands around 3445 cm^{-1}, 2934 cm^{-1} and 1707 cm^{-1} (OH, CH, and carboxyl related vibrations). After two washing steps, SC spectral features are barely visible evidencing efficient desorption of physisorbed surfactant and hence a possible strategy to widely remove the stabilizer.

Starting from a similarly exfoliated MoS_2 dispersion in SDS, surfactant related bands at 2922 cm^{-1}, 1468 cm^{-1}, 1249 cm^{-1}, 1222 cm^{-1} (CH, Sulfate and Alkyl-backbone) can clearly be identified. They can systematically be reduced by iterative washing with water (figure 3(B)). Although it is not possible to make a discrete quantification of MoS_2 surface coverage by surfactant at this stage due to different oscillator strengths of the vibrational modes of the organic molecules, the clear presence of the SDS after washing with water demonstrates that this surfactant is more difficult to remove. Further, it confirms that DRIFT spectroscopy in the MIR-FIR can be a fast and

effective tool for detecting organic residues in MoS_2 nanosheet samples that have been exfoliated using surfactants.

To avoid surfactant impurities in the first place, many groups in the field tend to exfoliate in pure solvents, with NMP being a prominent example, as exfoliation/stabilization was found to be very efficient based on solution thermodynamics [31]. The high boiling point nature of this solvent is often considered a drawback for further processing [29]. However, it is unclear whether it can be easily removed from the surface. In figure 3(C), the DRIFT spectra after sonication-assisted LPE in NMP after transfer to water for freeze-drying (1 wash), as well as additional centrifugation-based washing with isopropanol are shown. The data clearly shows that the washing protocol with IPA is not sufficient to remove surface adsorbates even though NMP is miscible with IPA. In particular, the characteristic feature at $\sim$1667 cm^{-1} can still be discerned after 6x washing (SI figure S8). It is possible that NMP molecules undergo further degradation or additional reactions during sonication, which cannot be fully excluded [36]. We plan to address this in future work.

To avoid NMP as a solvent, other approaches include the use of solvent blends, such as alcohol/water mixtures for exfoliation [29, 32, 37]. Typically alcohol contents of less than 60% (v/v) IPA, i.e. rather in the range of 30%–40% (v/v) IPA seem to yield the best efficiency in exfoliation [32, 37]. In this work, a starting volume ratio of IPA/H_2O of 60/40 was utilized, as a container open to the environment was used for exfoliation and hence evaporation of solvents plays a role. From our experience, these conditions give stable dispersions, comparable in nanosheet dimensions and yield to surfactant exfoliation if centrifugation parameters are adjusted for the viscosity of the medium [35, 37]. As figure 3(D) shows, the MIR spectral range of common organic vibrations is bereft of features from the beginning, which can be rationalized by the volatile nature of the utilized solvents.

Within the studied solvent/stabilizer systems, it appears that low boiling point solvent blends are removed from the MoS_2 surfaces during drying, whereas water/surfactant systems require additional purification through washing with water. Surprisingly, the residues of the common solvent NMP cannot be removed through washing protocols that were successful for aqueous surfactants. The success or failure of such protocols, particularly in the case of NMP, can be effectively tracked using DRIFT spectroscopy.

2.4. Organic residues after EE

Besides solvent stabilization (rationalized with solution thermodynamics) and surfactants stabilizing nanosheet dispersions via Coulomb repulsion, polymers can also be used to stabilize such dispersions, primarily through steric repulsion [29]. This method is widely applied to stabilize MoS_2 nanosheets after EE, where polyvinyl pyrrolidone (PVP) is probably one of the most commonly used polymers, typically in conjunction with DMF as solvent [3, 17]. A significant advantage of EE is the ability to achieve high length-thickness aspect ratios of nanosheets [3]. This makes the samples suitable for printed electronics in contrast to LPE nanosheets [3, 38, 39]. However, residual adsorbates can lead to unintentional doping and can cause issues with device fabrication. It is thus important to understand whether and how surface adsorbates, for example through dispersing the swollen crystal after electrochemical intercalation in DMF/PVP, can be efficiently removed.

In addition to the stabilizing agent, the intercalant also plays a crucial role in EE of MoS_2, as evidenced by literature, which shows clear differences in degree of exfoliation, i.e. nanosheet thickness depending on the intercalant [3, 40]. Both the intercalant, solvent and polymer are potential doping agents that might influence the targeted electrical properties towards a device application [41, 42]. Given this assumption, literature protocols for nanosheet processing already include washing procedures (e.g. by centrifugation or filtration) and/or annealing at high temperature [3, 17, 43]. However, maintaining the given nanosheet size and thickness distribution upon filtration is challenging, and annealing can lead to 2D material degradation [44, 45]. Therefore, centrifugation was the purification method of choice in this work. Obtaining a reliable spectroscopic measure for successful adsorbent removal is often difficult, which is why IR spectroscopy, in combination with UV–VIS, is utilized here. The specimens for IR were obtained from freeze-dried aqueous dispersions, and UV–VIS extinction spectra were measured in water in all cases.

We will focus on two batches of EE MoS_2 produced by distinct protocols in literature [3, 40]. The main difference is the intercalant used-Tetrapropylammonium Bromide (TPrABr) and Tetraheptylammonium Bromide (THepABr)- albeit some other parameters such as applied voltage are also different. Both samples have in common, that the intercalated MoS_2 crystals are immersed in a mixture of DMF/PVP for the delamination by mild bath sonication. In literature, it is described that the protocol using THepABr [40] yields thinner sheets on average than the protocol with TPrABr [3]. In figure 4(A+B) UV–VIS spectra of MoS_2 dispersions from the two different EE approaches are shown. The black trace corresponds to the dried MoS_2 sample, prepared by exfoliating the intercalated crystal in DMF/PVP, followed by transfer to H_2O via centrifugation and subsequent freeze-drying. The spectra show the characteristic excitonic features of MoS_2

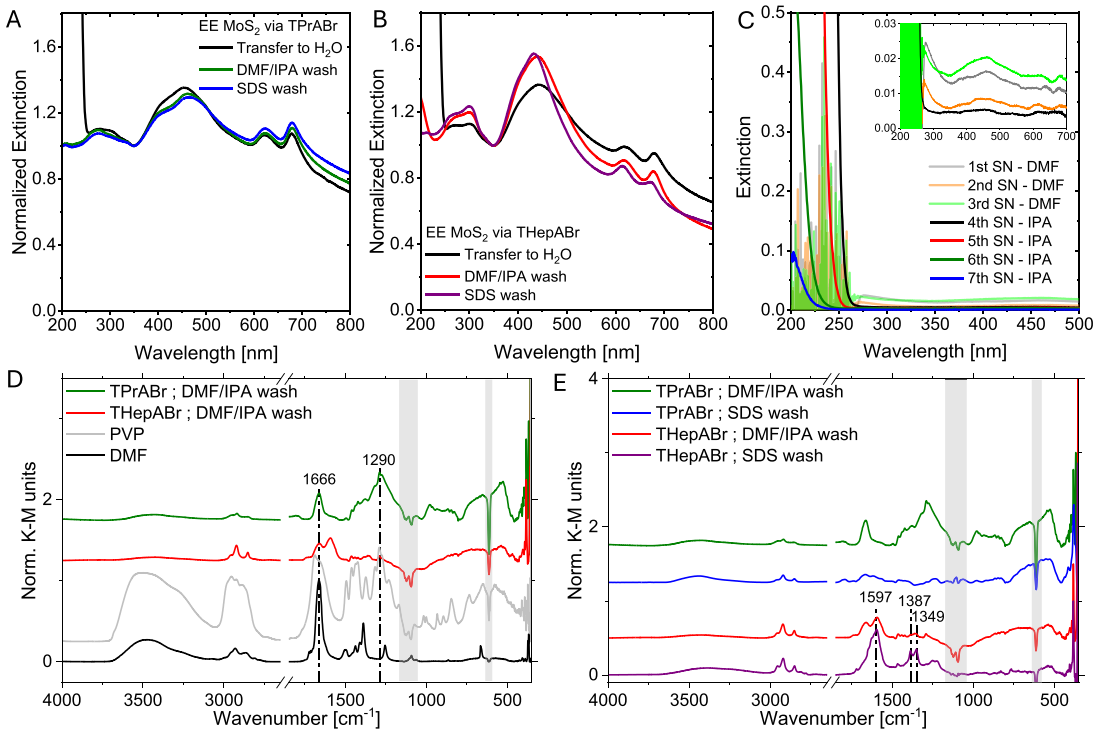

Figure 4. A+B) UV–VIS extinction spectra of MoS_2 dispersions after different washing protocols. (A) From EE in acetonitrile using TPrABr, (B) From EE in acetonitrile using THepABr. (C) UV–VIS extinction spectra of supernatants (SN) of TPrABr-MoS_2 washing with DMF/IPA and solvent transfer. D+E) Measured DRIFT spectra in mid-infrared of EE MoS_2-For reference, PVP and DMF were also mixed with CsI. For these references, normalization was done to 1666 cm^{-1} rather than the shear mode of MoS_2.

[46]. For LPE nanosheets, it is well understood how spectra change as a function of nanosheet thickness [47, 48] which influences the energy of the excitonic transitions and lateral size through edge effects [4, 48] and light scattering [4, 49]. This lead to the development of spectroscopic metrics to quantify nanosheet layer number and lateral size based on extinction spectra [22] (as used above to determine layer number). For EE MoS_2, the optical extinction spectra were also observed to differ for different production techniques, but were thus far not quantitatively linked to nanosheet dimension. Nonetheless, we attribute differences in the extinction spectra of as-obtained EE MoS_2 (black traces in figure 4(A+B)) to differences in nanosheet dimensions. In addition to the excitonic features, a sharp onset is observed in the UV-region (<250 nm which is attributed to residual DMF/PVP).

Both samples were subjected to centrifugation based washing using different protocols: On the one hand a literature-based washing protocol was tested, using DMF first to lower the PVP content and then IPA [3], a miscible solvent, that should remove residual DMF. On the other hand an adapted ligand-exchange approach was tested with the idea of exchanging the PVP with a different ionic stabilizer [50]. Here, SDS (2 g l^{-1}) was tested, as it was found above (figure 3(B)) that this surfactant can be removed after contact with MoS_2 and can be easily detected with IR spectroscopy. Binding interactions between PVP and SDS in solution as polymer-surfactant complexes have been previously reported, and binding competition to the polymer between SDS sulfate groups and OH groups (in the case of naphthol) has been suggested making SDS a reasonable choice [51]. The extinction spectra of the 'purified' MoS_2 samples are included in figure 4(A+B). We found that the number of washing cycles required to remove the majority of physisorbed DMF/PVP depends on the specific EE MoS_2 dispersion used. This can be followed through the measurement of the extinction spectra of the supernatants, that is typically discarded. Ideally, these should not show characteristic features of MoS_2, but contain the organic residues that are removed. A set of supernatant spectra for TPrABr-MoS_2 washed subsequently with DMF and IPA are shown in figure 4(C). For other datasets see figure S9. Due to the absorbance of DMF in the UV-region, this spectral region is not accessible for the first washing cycles with DMF (3 in this case). However, after subsequent washing with IPA, the supernatant spectra show the absorbance onset in the UV-region which gradually decreases. We use this to decide how many washing cycles are required, which is typically 5–7. The thus obtained MoS_2 dispersions were considered as 'purified'.

The extinction spectra of the purified dispersions show that the onset in the UV-region observed in the as-exfoliated samples has widely disappeared so

we attribute it to organic surface adsorbates from DMF/PVP and their successful removal. Other than that, for the TPrABr based sample (figure 4(A)), the washing protocols only lead to minor changes in the excitonic features. This would be expected for samples with similar nanosheet dimensions. In contrast, the THepABr based sample (figure 4(B)), a sharpening of excitonic features—especially of the C Exciton—can be observed after both washing procedures. It seems unreasonable that this is due to changes in nanosheet dimensions on washing, as the procedure involves centrifugation-based sedimentation of all nanosheets followed by agitation with fresh solvent which should not alter nanosheet size/thickness. Hence, this change must have a different origin. We observed that even more extensive washing results in aggregation, so it is possible that aggregation has already occurred to some extent in these samples. If that was the case, we would expect the nonresonant scattering background (>700 nm) to change, as the scattering exponent is related to the nanosheet (projected) area which is effectively increased in aggregates. However, changes in the scattering background are relatively minor. With nanosheet size effects and aggregation excluded, we suggest that the changes in the spectral shape after removal of the DMF/PVP is related to some form of solvatochromism, i.e. an alteration of the dielectric environment through removal of the surface adsorbates. Given that doping is known to reduce the oscillator strength of excitons, as also observed for MoS_2 under bias in transistors [52], a sharpening of the excitonic features is indicative of lower doping levels. Overall, the UV–VIS spectra qualitatively confirm the successful removal of organic residues through the centrifugation-based washing.

To gain further insights into the type of adsorbent and evaluate the effectiveness of purification protocols, IR spectroscopy was performed using freeze-dried powders from the above described dispersions (figure 4(D+E)). In figure 4(D), the normalized DRIFT spectra of EE MoS_2 washed subsequently with DMF and IPA are shown in comparison to DRIFT spectra of PVP and DMF (scaled to similar intensities). The literature-established washing protocol using DMF/IPA leaves the MoS_2 in case of the TPrABr-based exfoliation with residues that resemble a superposition of vibrations of DMF and PVP (green trace figure 4(D)). In comparison to as-obtained EE MoS_2, the vibrational modes of DMF and PVP are significantly reduced (see SI figure S10), confirming successful, but not complete removal of DMF and PVP. The purified sample from the THepABr-based exfoliation leads to a residual vibration resembling the C=O vibration of DMF around 1666 cm^{-1} as well as a new vibration observed at 1597 cm^{-1}. This band at this stage could not be attributed to any of the solvents, polymers or intercalants (see figures 4(D) and S11). Notably, when performing the SDS-based washing protocol on both MoS_2 dispersions obtained from EE, it appears that the residues are removed more efficiently from the TPrABr-based exfoliation MoS_2 resulting in a spectrum that shows no distinct features in the MIR (blue and green trace in figure 4(E)). We conclude that surface purification was effective in this case. For the THepABr-based dispersion, new bands at 1597, 1387, and 1349 cm^{-1} are observed (red and purple trace in figure 4(E)). It is worth mentioning that the band is at 1597 cm^{-1} was also present in the DMF/IPA-based washing of this material.

Since chemical compounds added in the production process (intercalant, solvent, stabilizer) cannot explain these features, other environmental factors must be considered. MoS_2 from different production techniques has been found to be particularly susceptible to adsorption of hydrocarbons used during sample preparation, even in solvent-free approaches such as mechanical exfoliation or chemical vapor deposition [2]. While very small amounts of these hydrocarbons require highly resolved techniques such as TOF-SIMS, larger amounts can be detected with techniques such as XPS or Raman spectroscopy. The latter is very well understood for a broad range of carbon-based planar nanomaterials, including ideal graphene [53], graphene with different degrees of defects [54] and nanographenes like C216 [55] as well as individual polycyclic aromatic compounds [56]. Interestingly, the bands associated with these nanographenes appear in similar ranges as the IR bands observed in the SDS-washed MoS_2 samples (G band at ~1600 cm^{-1}, D-bands at 1320–1370 cm^{-1}). Further, a few reports on IR Spectroscopy of nanocarbons can be found which align with the above measured bands in these compounds [57, 58] confirming that the vibrations are also IR active. While this is an interesting observation, the origin of the species could not be found. It is worth noting that, only centrifugation vials (see methods) and ambient air come into contact with the dispersions (assuming that glass containers and pipettes do not contain carbonaceous species). Nonetheless, the larger relative intensity of these unassigned bands after SDS washing compared to DMF/IPA washing could suggest the improved removal of other molecules on the surface leaving MoS_2 fully exposed to the environment and thus accessible to the adsorption of hydrocarbons from the environment. For TPrABr-based samples the effect might not be observed, as nanosheets in the case of exfoliation using THepABr are thinner on average [40] compared to the samples from TPrABr, and hence have the larger effective MoS_2 surface area. Regardless of these species, we note that DRIFT Spectroscopy clearly shows a successful removal of the DMF/PVP surface adsorbates through the washing protocols, in particular the SDS replacement protocol. However,

much more extensive washing is required than for the removal of small molecule surfactants on LPE nanosheets.

3. Conclusion

In summary, we have developed a method based on DRIFT spectroscopy, incorporating sample preparation via freeze-drying, to monitor organic residues on MoS_2 nanosheets produced by different exfoliation strategies in the liquid phase. The theoretically predicted vibrational modes of MoS_2 are experimentally confirmed including shifts and changes in relative intensities with layer number in the mono and few-layered regime (1–10 layers). The protocol can potentially be applied to other 2D materials with IR active vibrational modes in the FIR. As such, there is scope to determine average nanosheet dimensions in an ensemble based on the IR spectra. This can be advantageous, as IR spectra are easier to predict and thus to interpret than resonant Raman spectra.

In addition, we could successfully track the removal of adsorbates in centrifugation-based washing through the IR studies. Since organic residues show IR active vibrations in the MIR with no spectral overlap with the signature of the nanosheets in the FIR, a normalization to the Mo–S vibrations allowed a direct comparison across samples. Compared to MoS_2 stabilized in aqueous media by small molecule surfactants such as SC and SDS (2 g l^{-1}), MoS_2 produced from LPE in NMP or EE and subsequent dispersion in DMF with PVP stabilizer (1 g l^{-1}, respectively) are significantly more difficult to purify. In the former case, three steps of sedimentation through centrifugation and redispersion in water were sufficient to remove the surfactant. For LPE MoS_2 in NMP and EE MoS_2, surface adsorbates were still detected after >7 times washing (with IPA and IPA/DMF). Nevertheless, the effectiveness of each purification method—be it established ones or newly tested ligand-exchange approaches—could be evaluated with DRIFT. This is an essential capability when precise control over surface composition or chemical functionalization is required for targeted (device) applications. The exceptionally clean IR spectra obtained from exfoliation in IPA/H_2O highlight the benefits of avoiding non-volatile organic compounds during processing, suggesting a valuable route for improving material quality from the start. Beyond merely detecting the presence of organic molecules on the 2D material surfaces, our method can also partially monitor molecular modifications during processing, as exemplified by the identification of cholic acid from exfoliation in H_2O/SC and the emergence of new vibrational features in the NMP spectra after MoS_2 exfoliation in this solvent.

Overall, this work provides a robust framework for evaluating the impact of each step in the liquid processing of 2D materials using low-cost benchtop equipment. It supports improved purification strategies, enables controlled functionalization, and deepens our understanding of molecular-level changes during exfoliation—ultimately contributing to higher-quality nanomaterials for use in electronic, chemical, and sensing devices. Future work will be directed towards a quantification of the degree of surface coverage based on DRIFT. In principle, precise quantification of impurities and chemical modifications on 2D material scaffolds can be achieved by titration or thermogravimetric analysis (TGA) [59, 60]. While titration targets specific functional groups or adsorbed species, TGA is particularly effective for modified MoS_2 [6]. Coupled with IR or mass spectrometry, TGA enables both quantitative and qualitative identification of impurities and modifications and can be used to establish calibration curves for DRIFT measurements to achieve a full quantification. This is advantageous, as DRIFT is low-cost, robust to perform and requires relatively small amounts of material (0.5–1 mg).

4. Methods

DFT calculations: first-principles DFT calculations were carried out using the Quantum ESPRESSO [61–63]distribution through the AiiDA [63–65] infrastructure. In particular, IR and phonon calculations were performed using the aiida-vibroscopy plugin [20] that employs a finite displacements [66, 67] and finite fields [68] approach. The initial multilayer structures were generated by stacking 2H-phase MLs with an interlayer distance of 3 Å and a base vacuum of 30 Å plus an additional 5 Å for each layer to avoid interactions among periodic replicas. Before performing the vibrational spectra calculations, the positions of the atoms in the unit cell and the lattice vectors were optimized for all the structures until the total energy, forces acting on atoms, and hydrostatic pressure are respectively less than 10^{-6} Ry $atom^{-1}$, 10^{-4} Ry $Bohr^{-1}$, and 0.5 kbar. We used the rVV10 prescription [69] for the DFT functional and pseudopotentials from the SSSP PBE precision library (version 1.3) [70]. The kinetic wavefunction and charge density cutoffs are set to the recommended values of the SSSP library [70, 71]. The Brillouin zone is sampled uniformly with a Γ-centred 16x16x1 ***k***-points mesh. Finite differences are carried out using a default 0.01 Å displacement distance for the calculation of the interatomic force constants, and an automated selection of the finite electric field as proposed in [20] with a 2nd-order numerical accuracy to calculate the Born effective charge tensors Z^*_{Iij} (I is the atom index, i and j refer to the three directions in space)

needed for the calculation of the oscillator strength of the phonon modes. By following the derivation of [72]. we describe the layers as in close contact with the dielectric medium, CsI, with dielectric constant $\in_{CsI} = 5.65,$ and calculate the powder IR spectra as the dissipated power by the incoming electromagnetic radiation:

$$W(\omega) \propto \omega \ \mathrm{Im}\left[\in(\omega) - \frac{\boldsymbol{n}\cdot[\in(\omega) - \in_{CsI}\boldsymbol{I}]^2\cdot\boldsymbol{n}}{3[\boldsymbol{n}\cdot\in(\omega)\cdot\boldsymbol{n}]}\right],.$$

where $\boldsymbol{I}$ is the identity matrix, $\boldsymbol{n}$ is a unitary vector orthogonal to the layers surface, $\in(\omega)$ is the low frequency imaginary dielectric tensor of the layers, and $\in(\omega) = 1/3\ Tr \in(\omega)$. The imaginary dielectric function is described by an oscillator model:

$$\in(\omega) = \in_{ij}(\omega) = \in_{ij}^{\infty} + \frac{4\pi}{\Omega}\sum_{\nu}\frac{\bar{Z}_i^{\nu}\bar{Z}_j^{\nu}}{\omega^2 - \omega_{\nu}^2 - \mathrm{i}\gamma\omega},$$

where Ω is the unit cell volume, $\in_{ij}^{\infty}$ is the high-frequency (i.e. purely electronic) dielectric tensor, ν is the vibrational mode index, ω_{ν} the mode frequency, γ the damping coefficient (here set to 4 cm^{-1}), and $\bar{Z}_i^{\nu}$ is the oscillator strength. The latter is calculated from the effective charges and the phonon eigenvectors u_{Ij}^{ν} —obtained by diagonalizing the interatomic force constant matrix—as follows (see also [20] and references within):

$$\bar{Z}_i^{\nu} = \sum_{Ij} Z_{Iij}^{*}\frac{u_{Ij}^{\nu}}{\sqrt{M_I}},$$

where M_I is the mass of atom I. We note that longitudinal optical (LO) modes are not accounted for in the IR spectra, as they are not detectable in a near-to-normal experimental setup, typically requiring special experimental setups, such as angle resolution and polarized light [73]. Moreover, the LO-TO splitting in few layers MoS_2 is expected to be small [74]. We also emphasize that, if their comparison to experiments would be viable, a dimensional-specific treatment of the long-range electrostatic interactions, needed to obtain LO modes in the long-wavelength limit, would be required for low-dimensional materials [74, 75].

Explicitly accounting for the dielectric environment enhances the absorption associated with out-of-plane modes. This follows directly from the analytic form of $W(\omega)$: phonons whose oscillator strengths are aligned with the surface normal $\boldsymbol{n}$ are amplified by a factor proportional to the dielectric constant of the surrounding CsI medium. If this effect is neglected, the computed out-of-plane modes become barely discernible relative to the bulk response, in contrast with experiment. Our modeling therefore better reflects the measurement conditions, and we recommend using it for quantitative comparison with data—for example, to infer the number of layers from relative peak intensities when a clear trend could be resolved.

Liquid Phase Exfoliation: In an 80 ml screw cap vial the powders of the respective transition metal dichalcogenide (1.6 g, 20 g l^{-1}, MoS_2, Sigma-Aldrich 69860) and surfactant (0.64 g, 8 g l^{-1}, SC C1254 or sodium dodecyl sulfate L3771) were mixed with deionized water (80 ml). For exfoliation in other solvents—NMP (Carl Roth, 4306.1) or 60/40 mixtures of 2-Propanol (59300) and water (Stakpure Omniapure UV-TOC)—no surfactant was used, and the volume of the solvent was kept the same. After transferring the dispersion into a stainless-steel container of adequate volume, the container was fixed into a holder in a water chilling setup (temp.: 5 °C). The cooling water level was carefully adjusted to the filling height of the metal container. The tip of the tip sonicator (Sonics VCX 500 (500 watts) with a horn tip purchased from Sigma-Aldrich) was placed about 1 cm above the bottom level of the metal container in a central position. During tip sonication the ultrasonication converter was cooled with compressed air. Typically, the settings for the initial sonication were 60% amplitude with pulse durations of about 6 s on-pulse and 4 s off-pulse and an absolute sonication time of 1 h. The dispersion obtained thereafter was transferred into centrifugation tubes and centrifuged at 6000 rpm for 2 h. Then the supernatant, containing impurities, was removed and the sediment was redispersed into ∼80 ml of surfactant solution (2 g l^{-1}) or solvent respectively. Then the dispersion is transferred back into the steel-container and another tip-sonication with 60% amplitude, pulse durations of 6 s on-pulse and 4 s off-pulse and an absolute sonication time of 7 h is started (usually overnight).

Size Selection: The size selection protocol is based on centrifugation (2 h for each step) and the subsequent separation of supernatant and sediment. The supernatant is transferred to new centrifugation tubes for centrifugation at higher speeds. The sediment obtained after the first centrifugation (2000 rpm) is discarded, as it contains mostly unexfoliated material. Sediments after the next centrifugation steps are collected (3000 rpm, 6500 rpm, 9200 rpm, 16k rpm, 21k rpm). The sediments were redispersed in water.

For studies of adsorbent removal instead of full cascade, it was reduced to a fraction trapped between 2240–5000 rpm in water. For other solvents the speeds were adapted to account for the different viscosities (2950–6600 rpm in NMP, 4490 rpm—10 krpm in IPA/H_2O) according to [35].

The centrifugation steps were carried out using 2 different types of centrifuges. All experiments were carried out at 15 °C if not stated otherwise. A Hettich MIKRO 220 R tabletop centrifuge was used for accelerations up to 3000 rpm.

For larger amounts of dispersion, the above-mentioned centrifuge was used for accelerations up to 3000 rpm with a 1016 type rotor and VWR High-Performance Centrifuge Tubes with Flat Caps

(Polypropylene, 50 ml) with a filling height of about 20 ml. Centrifugation at higher speeds (>6000 rpm) was accomplished by a Beckman Coulter Avanti J-26 XP centrifuge with 15 mL Beckman Coulter polyethylene tubes with a filling height of about 10 ml in a JA-25.15 rotor.

Studies on purification of electrochemically exfoliated MoS_2: EE of MoS_2 with tetrapropylammonium bromide was done as derived from methods described by Carey *et al* [3]. After the final decanting of the dispersion in IPA, the expanded 2D crystal (natural origin, Krupka, Czech Republic) was bath-sonicated (Fisherbrand 112xx series) in 1 g l^{-1} poly(vinylpyrrolidone) (PVP, molecular weight∼40000) in DMF for 5 min. EE of MoS_2 with the intercalant tetraheptylammonium bromide was performed according to Neilson *et al* [40] with the following modifications: The available electrochemical setup was a cell with $V = 30$ ml and an anode of glassy carbon. Process time was reduced to 30 min and the exact concentration of the intercalant THepABr was 10.8 g l^{-1}. Sonication was done in 1 g l^{-1} PVP in DMF. A centrifugation at 100 rpm for 3 h was performed in a swinging bucket rotor (Avanti, JS-13.1) to remove unexfoliated material. As no extinction coefficient was available to determine the amount of material for the further experiments, 2 ml of dispersions with an extinction of 4.85 were used (calculated, correcting for dilution in UV–VIS experiment and cuvette path length). For transfer into other solvent/stabilizer systems dispersions were centrifuged for 1 h at 15k rpm and supernatants were monitored via UV–VIS spectroscopy. For reference, materials were directly transferred to water (figure S10). For other samples, a washing protocol with 2x DMF and 2x IPA was applied to remove PVP and finally DMF. To improve removal of residual adsorbents, the initial dispersions of MoS_2 in DMF/PVP were centrifuged and redispersed 2x in SDS (2 g l^{-1}) and to remove SDS 2x in water.

UV–VIS spectroscopy: Extinction spectra of dispersions were recorded in 0.4 × 1 cm^2 quartz cuvettes using a Agilent Cary 60 U/VIS absorption spectrometer with wavelength increments of 0.5 nm. Baseline measurements were performed using the pure solvent of the respective nanosheet dispersions. From these spectra average flake metrics as well as the mass concentrations were extracted via a method developed by Goldie *et al* [22] For further processing a volume of each dispersion was processed to meet an amount of about 1.2 mg, also calculated using this tool.

Sample preparation for IR spectroscopy: Required volumes of dispersions were diluted to 6 ml and distributed to four 1.5 ml Eppendorf SafeLock Tubes. For all size fractions (see figure 2; except the smallest one) the obtained dispersions were centrifuged at 30 kg three times and the sediment each time redispersed with water. For the smallest fraction Beckman Coulter 1.5 ml polypropylene tubes were used and Avanti J-26 XP was used at 21 000 rpm using a JA-25.15 rotor with the necessary adapters.

To obtain more data in the range of relatively thin nanosheets, ML enrichment was performed with fraction 9.2–16k rpm by centrifuging at 2.5k rpm for 15 h. Analogous UV–VIS evaluation and washing via centrifugation and redispersion lead to additional data for the plots in this manuscript.

Stepwise washing using average size nanosheets as shown in figure 3 was done by centrifuging 2 h at 7200 rpm for samples in water, 10 krpm for samples in NMP, 12 krpm for samples in IPA/H_2O (60/40) respectively. Redispersion was done using water, except for the washing of NMP based samples, where IPA was used. The final redispersion step was always done with water to facilitate freeze-drying.

The obtained aqueous dispersions were then frozen in liquid nitrogen and then freeze-dried in a Zirbus VaCo 2 at 0.1 mbar for 24 h. The obtained powders (∼0.5–1 mg) were mixed with CsI (∼ 100 mg; ThermoFisher 10022) in an agate mortar and then transferred to the microbeakers of a PerkinElmer Spectrum 3 FTIR Spectrometer equipped with a diffuse Reflectance sampling accessory. The autofocus function was used for Background measurement (microbeaker with pure CsI) with the same procedure for sample measurements. Automatic CO_2/H_2O correction was done in the MIR region. In the MIR range at least 50 spectra were collected and averaged in the FIR 100. Spectra were acquired with 1 cm^{-1} data point increments (achieved by setting the internal resolution to 4 cm^{-1}). Scan speed was 0.2 cm s^{-1}. After Kubelka–Munk transformation and manual baseline subtraction, spectra were normalized to the shear mode of MoS_2 at 384 cm^{-1}.

Data availability statement

The data cannot be made publicly available upon publication because they are not available in a format that is sufficiently accessible or reusable by other researchers. The data that support the findings of this study are available upon reasonable request from the authors.

Supplementary material available at https://doi.org/10.1088/2053-1583/ae1148/data1.

Acknowledgments

J.N.C., Z.S., N.M. and C.B. acknowledge funding from the European Union through the 2D-PRINTABLE project (GA-101135196). L.B. and

N.M. gratefully acknowledge support from the Deutsche Forschungsgemeinschaft (DFG) under Germany's Excellence Strategy (EXC 2077, No. 390741603, University Allowance, University of Bremen) and Lucio Colombi Ciacchi, the host of the 'U Bremen Excellence Chair Program'. N.M. acknowledges support by the NCCR MARVEL, a National Centre of Competence in Research, funded by the Swiss National Science Foundation (Grant Number 205602). T.C. acknowledges funding by the Royal Society—Research Ireland University Research Fellowship (Project THINK). K.S. acknowledges financial support by the Deutsche Forschungsgemeinschaft (DFG) through CRC-1415–417590517. Z.S. was supported by ERC-CZ program (project LL2101) from Ministry of Education Youth and Sports (MEYS) and by the project Advanced Functional Nanorobots (reg. No. CZ.02.1.01/0.0/0.0/15_003/0000444 financed by the EFRR).

Author contributions

Tim Nowack 0000-0001-6349-8617
Conceptualization (supporting), Data curation (lead), Formal analysis (lead), Investigation (equal), Methodology (lead), Visualization (equal), Writing – original draft (lead), Writing – review & editing (supporting)

Lorenzo Bastonero 0000-0001-9374-1876
Data curation (supporting), Formal analysis (supporting), Investigation (equal), Writing – review & editing (supporting)

Timm Knickrehm 0000-0002-3502-6310
Investigation (supporting), Writing – review & editing (supporting)

Tian Carey 0000-0001-8697-9421
Investigation (supporting), Writing – review & editing (supporting), Funding acquisition (equal)

Oran Cassidy 0000-0002-1136-6708
Investigation (supporting), Writing – review & editing (supporting)

Jonathan N Coleman 0000-0001-9659-9721
Funding acquisition (equal), Resources (supporting), Supervision (supporting), Writing – review & editing (supporting)

Zdenek Sofer 0000-0002-1391-4448
Investigation (supporting), Writing – review & editing (supporting), Funding acquisition (equal)

Kevin R Synnatschke 0000-0001-7018-9396
Investigation (supporting), Writing – review & editing (supporting), Funding acquisition (equal)

Nicola Marzari 0000-0002-9764-0199
Funding acquisition (equal), Resources (supporting), Supervision (supporting), Writing – review & editing (supporting)

Claudia Backes 0000-0002-4154-0439
Conceptualization (lead), Funding acquisition (equal), Methodology (supporting), Resources (lead), Supervision (lead), Visualization (equal), Writing – review & editing (lead)

References

[1] Novoselov K S, Geim A K, Morozov S V, Jiang D, Zhang Y, Dubonos S V, Grigorieva I V and Firsov A A 2004 Electric field effect in atomically thin carbon films *Science* **306** 666–9
[2] Tilmann R, Bartlam C, Hartwig O, Tywoniuk B, Dominik N, Cullen C P, Peters L, Stimpel-Lindner T, McEvoy N and Duesberg G S 2023 Identification of ubiquitously present polymeric adlayers on 2D transition metal dichalcogenides *ACS Nano* **17** 10617–27
[3] Carey T *et al* 2023 High-mobility flexible transistors with low-temperature solution-processed tungsten dichalcogenides *ACS Nano* **17** 2912–22
[4] Backes C *et al* 2014 Edge and confinement effects allow *in situ* measurement of size and thickness of liquid-exfoliated nanosheets *Nat. Commun.* **5** 4576
[5] Hanlon D *et al* 2015 Liquid exfoliation of solvent-stabilized few-layer black phosphorus for applications beyond electronics *Nat. Commun.* **6** 8563
[6] Knirsch K C *et al* 2015 Basal-plane functionalization of chemically exfoliated molybdenum disulfide by diazonium salts *ACS Nano* **9** 6018–30
[7] Yang L *et al* 2014 Chloride molecular doping technique on 2D materials: WS_2 and MoS_2 *Nano Lett.* **14** 6275–80
[8] Kiriya D, Tosun M, Zhao P, Kang J S and Javey A 2014 Air-stable surface charge transfer doping of MoS_2 by benzyl viologen *J. Am. Chem. Soc.* **136** 7853–6
[9] Liu J, Li B and Li Q 2022 Two-dimensional doped materials *Magnetochemistry* **8** 172
[10] Santos V P, van der Linden B, Chojecki A, Budroni G, Corthals S, Shibata H, Meima G R, Kapteijn F, Makkee M and Gascon J 2013 Mechanistic insight into the synthesis of higher alcohols from syngas: the role of K promotion on MoS_2 catalysts *ACS Catal.* **3** 1634–7
[11] Chen X, Berner N C, Backes C, Duesberg G S and McDonald A R 2016 Functionalization of two-dimensional MoS_2 : on the reaction between MoS_2 and organic thiols *Angew. Chem., Int. Ed. Engl.* **55** 5803–8
[12] Chen X *et al* 2021 Covalent bisfunctionalization of two-dimensional molybdenum disulfide *Angew. Chem. Int. Ed.* **60** 13484–92
[13] Tuci G *et al* 2018 Surface engineering of chemically exfoliated MoS_2 in a "click": how to generate versatile multifunctional transition metal dichalcogenides-based platforms *Chem. Mater.* **30** 8257–69
[14] Molina-Sánchez A, Hummer K and Wirtz L 2015 Vibrational and optical properties of MoS_2: from monolayer to bulk *Surf. Sci. Rep.* **70** 554–86
[15] Backes C, Berner N C, Chen X, Lafargue P, LaPlace P, Freeley M, Duesberg G S, Coleman J N and McDonald A R 2015 Functionalization of liquid-exfoliated two-dimensional 2H-MoS_2 *Angew. Chem. Int. Ed.* **54** 2638–42
[16] Pimenta M A, Del Corro E, Carvalho B R, Fantini C and Malard L M 2015 Comparative study of raman spectroscopy

in graphene and MoS_2-type transition metal dichalcogenides *Acc. Chem. Res.* **48** 41–47
[17] Lin Z *et al* 2018 Solution-processable 2D semiconductors for high-performance large-area electronics *Nature* **562** 254–8
[18] Eidsvåg H, Rasukkannu M, Velauthapillai D and Vajeeston P 2021 In-depth first-principle study on novel MoS_2 polymorphs *RSC Adv.* **11** 3759–69
[19] Pizzi G, Milana S, Ferrari A C, Marzari N and Gibertini M 2021 Shear and breathing modes of layered materials *ACS Nano* **15** 12509–34
[20] Bastonero L and Marzari N 2024 Automated all-functionals infrared and Raman spectra *npj Comput. Mater.* **10** 55
[21] Backes C *et al* 2016 Production of highly monolayer enriched dispersions of liquid-exfoliated nanosheets by liquid cascade centrifugation *ACS Nano* **10** 1589–601
[22] Kubetschek N, Backes C and Goldie S 2024 Algorithm for reproducible analysis of semiconducting 2D nanomaterials based on UV-VIS spectroscopy *Adv. Mater. Interfaces* **11** 2400311
[23] Muscuso L, Cravanzola S, Cesano F, Scarano D and Zecchina A 2015 Optical, vibrational, and structural properties of MoS_2 nanoparticles obtained by exfoliation and fragmentation via ultrasound cavitation in isopropyl alcohol *J. Phys. Chem. C* **119** 3791–801
[24] Liang Q, Dwaraknath S and Persson K A 2019 High-throughput computation and evaluation of raman spectra *Sci. Data* **6** 135
[25] Li Y, Lee D K J, Cai P, Zhang Z, Gorai P and Canepa P 2024 A database of computed Raman spectra of inorganic compounds with accurate hybrid functionals *Sci. Data* **11** 105
[26] Bagheri M and Komsa H-P 2023 High-throughput computation of Raman spectra from first principles *Sci. Data* **10** 80
[27] Pazhedath A, Bastonero L, Marzari N and Simoncelli M 2024 First-principles characterization of thermal conductivity in $LaPO_4$-based alloys *Phys. Rev. Appl.* **22** 024064
[28] Gebreyesus G, Bastonero L, Kotiuga M, Marzari N and Timrov I 2023 Understanding the role of Hubbard corrections in the rhombohedral phase of $BaTiO_3$ *Phys. Rev. B* **108** 235171
[29] Backes C 2021 *12—Production of Graphene and Other Two-dimensional Nanosheets by Liquid Phase Exfoliation* (*Graphene*) 2nd eds, ed V Skakalova and A B Kaiser (Woodhead Publishing) pp 251–314
[30] Karger L, Synnatschke K, Settele S, Hofstetter Y J, Nowack T, Zaumseil J, Vaynzof Y and Backes C 2021 The role of additives in suppressing the degradation of liquid-exfoliated WS_2 monolayers *Adv. Mater.* **33** 2102883
[31] Coleman J N *et al* 2011 Two-dimensional nanosheets produced by liquid exfoliation of layered materials *Science* **331** 568–71
[32] Halim U, Zheng C R, Chen Y, Lin Z, Jiang S, Cheng R, Huang Y and Duan X 2013 A rational design of cosolvent exfoliation of layered materials by directly probing liquid–solid interaction *Nat. Commun.* **4** 2213
[33] Ott S, Wolff N, Rashvand F, Rao V J, Zaumseil J and Backes C 2019 Impact of the MoS_2 starting material on the dispersion quality and quantity after liquid phase exfoliation *Chem. Mater.* **31** 8424–31
[34] O'Neill A, Khan U, Nirmalraj P N, Boland J and Coleman J N 2011 Graphene dispersion and exfoliation in low boiling point solvents *J. Phys. Chem. C* **115** 5422–8
[35] Goldie S, Ott S, Dawson A, Starke T, Gabbett C, Vega V, Synnatschke K, Horn M, Coleman J N and Backes C 2025 Centrifugation theory revisited: understanding and modelling the centrifugation of 2D nanosheets (arXiv:2503.05111)
[36] Ou Y J, Wang X M, Li C L, Zhu Y L and Li X L 2017 The effects of alkali and temperature on the hydrolysis rate of n-methylpyrrolidone *IOP Conf. Ser.: Earth Environ. Sci.* **100** 012036
[37] Alzakia F I, Sun W, Pennycook S J and Tan S C 2020 Introducing normalized centrifugation for a more accurate thermodynamic analysis of molybdenum disulfide dispersions: a study on mixed solvents of alcohols and amines with water *ACS Appl. Mater. Interfaces* **12** 3096–103
[38] Kelly A 2025 *Junction Engineering in Solution-processed Nanosheet Networks* (Researchgate) 10.13140/RG.2.2.32828.55689
[39] Carey T S *et al* 2024 *A Portfolio of Electrochemically Exfoliated Two-Dimensional Materials: From Crystals and Simulations to Electronic Inks and Circuits* (Research Square) 10.21203/rs.3.rs-5319871/v1
[40] Neilson J *et al* 2024 Production of ultrathin and high-quality nanosheet networks via layer-by-layer assembly at liquid–liquid interfaces *ACS Nano* **18** 32589–601
[41] Wang Q H, Kalantar-Zadeh K, Kis A, Coleman J N and Strano M S 2012 Electronics and optoelectronics of two-dimensional transition metal dichalcogenides *Nat. Nanotechnol.* **7** 699–712
[42] Vega-Mayoral V, Backes C, Hanlon D, Khan U, Gholamvand Z, O'Brien M, Duesberg G S, Gadermaier C and Coleman J N 2016 Photoluminescence from liquid-exfoliated WS_2Monomers in poly(vinyl alcohol) Polymer Composites *Adv. Funct. Mater.* **26** 1028–39
[43] Liu N, Kim P, Kim J H, Ye J H, Kim S and Lee C J 2014 Large-area atomically thin MoS_2 nanosheets prepared using electrochemical exfoliation *ACS Nano* **8** 6902–10
[44] Yamamoto M, Einstein T L, Fuhrer M S and Cullen W G 2013 Anisotropic etching of atomically thin MoS_2 *J. Phys. Chem. C* **117** 25643–9
[45] Wu J, Li H, Yin Z, Li H, Liu J, Cao X, Zhang Q and Zhang H 2013 Layer thinning and etching of mechanically exfoliated MoS_2 nanosheets by thermal annealing in air *Small* **9** 3314–9
[46] Wilson J A and Yoffe A D 1969 The transition metal dichalcogenides discussion and interpretation of the observed optical, electrical and structural properties *Adv. Phys.* **18** 193–335
[47] Frisenda R *et al* 2017 Micro-reflectance and transmittance spectroscopy: a versatile and powerful tool to characterize 2D materials *J. Phys. D: Appl. Phys.* **50** 074002
[48] Synnatschke K, Cieslik P A, Harvey A, Castellanos-Gomez A, Tian T, Shih C-J, Chernikov A, Santos E J G, Coleman J N and Backes C 2019 Length- and thickness-dependent optical response of liquid-exfoliated transition metal dichalcogenides *Chem. Mater.* **31** 10049–62
[49] Yadgarov L, Choi C L, Sedova A, Cohen A, Rosentsveig R, Bar-Elli O, Oron D, Dai H and Tenne R 2014 Dependence of the absorption and optical surface plasmon scattering of MoS_2 nanoparticles on aspect ratio, size, and media *ACS Nano* **8** 3575–83
[50] Dong A, Ye X, Chen J, Kang Y, Gordon T, Kikkawa J M and Murray C B 2011 A generalized ligand-exchange strategy enabling sequential surface functionalization of colloidal nanocrystals *J. Am. Chem. Soc.* **133** 998–1006
[51] Saito S 1967 Solubilization properties of polymer-surfactant complexes *J. Colloid Interface Sci.* **24** 227–34
[52] Mak K F, He K, Lee C, Lee G H, Hone J, Heinz T F and Shan J 2013 Tightly bound trions in monolayer MoS_2 *Nat. Mater.* **12** 207–11
[53] Malard L M, Pimenta M A, Dresselhaus G and Dresselhaus M S 2009 Raman spectroscopy in graphene *Phys. Rep.* **473** 51–87
[54] Gustavo Cançado L, Gomes da Silva M, Martins Ferreira E H, Hof F, Kampioti K, Huang K, Pénicaud A, Alberto Achete C, Capaz R B and Jorio A 2017 Disentangling contributions of point and line defects in the Raman spectra of graphene-related materials *2D Mater.* **4** 025039
[55] Maghsoumi A, Beser U, Feng X, Narita A, Müllen K, Castiglioni C and Tommasini M 2021 Raman spectroscopy of holey nanographene C216 *J. Raman Spectrosc.* **52** 2301–16
[56] Cloutis E, Szymanski P, Applin D and Goltz D 2016 Identification and discrimination of polycyclic aromatic hydrocarbons using Raman spectroscopy *Icarus* **274** 211–30

[57] Fuente E, Menéndez J A, Díez M A, Suárez D and Montes-Morán M A 2003 Infrared spectroscopy of carbon materials: a quantum chemical study of model compounds *J. Phys. Chem. B* **107** 6350–9
[58] Bekhterev A N and Zolotarev V M 2007 Infrared diffuse reflection spectroscopy of vibration states in nanocarbons *Diam. Relat. Mater.* **16** 2093–7
[59] Ederer J, Janoš P, Ecorchard P, Štengl V, Bělčická Z, Šťastný M, Pop-Georgievski O and Dohnal V 2016 Quantitative determination of acidic groups in functionalized graphene by direct titration *React. Funct. Polym.* **103** 44–53
[60] Aliyev E, Filiz V, Khan M M, Lee Y J, Abetz C and Abetz V 2019 Structural characterization of graphene oxide: surface functional groups and fractionated oxidative debris *Nanomaterials* **9** 1180
[61] Giannozzi P *et al* 2009 QUANTUM ESPRESSO: a modular and open-source software project for quantum simulations of materials *J. Phys.: Condens. Matter* **21** 395502
[62] Giannozzi P *et al* 2017 Advanced capabilities for materials modelling with Quantum ESPRESSO *J. Phys.: Condens. Matter* **29** 465901
[63] Giannozzi P *et al* 2020 Quantum ESPRESSO toward the exascale *J. Chem. Phys.* **152** 154105
[64] Uhrin M, Huber S P, Yu J, Marzari N and Pizzi G 2021 Workflows in AiiDA: engineering a high-throughput, event-based engine for robust and modular computational workflows *Comput. Mater. Sci.* **187** 110086
[65] Huber S P *et al* 2020 AiiDA 1.0, a scalable computational infrastructure for automated reproducible workflows and data provenance *Sci. Data* **7** 300
[66] Togo A 2022 First-principles phonon calculations with phonopy and Phono3py *J. Phys. Soc. Japan* **92** 012001
[67] Togo A, Chaput L, Tadano T and Tanaka I 2023 Implementation strategies in phonopy and phono3py *J. Phys.: Condens. Matter* **35** 353001
[68] Umari P and Pasquarello A 2002 Ab initio molecular dynamics in a finite homogeneous electric field *Phys. Rev. Lett.* **89** 157602
[69] Sabatini R, Gorni T and de Gironcoli S 2013 Nonlocal van der Waals density functional made simple and efficient *Phys. Rev. B* **87** 041108
[70] Prandini G, Marrazzo A, Castelli I E, Mounet N and Marzari N 2018 Precision and efficiency in solid-state pseudopotential calculations *npj Comput. Mater.* **4** 72
[71] Bosoni E *et al* 2024 How to verify the precision of density-functional-theory implementations via reproducible and universal workflows *Nat. Rev. Phys.* **6** 45–58
[72] Balan E, Saitta A M, Mauri F and Calas G 2001 First-principles modeling of the infrared spectrum of kaolinite *Am. Mineral.* **86** 1321–30
[73] Brüesch P 1986 *Phonons: Theory and Experiments II* (Springer)
[74] Sohier T, Gibertini M, Calandra M, Mauri F and Marzari N 2017 Breakdown of optical phonons' splitting in two-dimensional materials *Nano Lett.* **17** 3758–63
[75] Rivano N, Marzari N and Sohier T 2023 Infrared-active phonons in one-dimensional materials and their spectroscopic signatures *npj Comput. Mater.* **9** 194